Marine Geology
December 2004; 213(1-4) : 323-342
http://dx.doi.org/10.1016/j.margeo.2004.10.012

Mechanical behaviour of unsaturated marine sediments: experimental and theoretical approaches

E. Vanoudheusden, N. Sultan* and P. Cochonat

IFREMER Brest, Departement de Geosciences Marines, Technopole de Brest-Iroise, B.P. 70, Plouzané F-29280, France

*: Corresponding author : Tel.: +33 2 98 22 42 59; fax: +33 2 98 22 45 70. nabil.sultan@ifremer.fr

Abstract: The COSTA target areas exhibit different slope failure events, which reflect different triggering mechanisms including gas hydrates dissociation. Gas hydrates stability law depends on temperature, pore pressure, gas chemistry, and pore water salinity. Any change in the equilibrium parameters may convert the hydrate to gas plus water, causing significant weakening of the sediment, and generating a rise of pore pressure. A significant consequence of the hydrate melting is the gas production, which alters significantly the behaviour and mechanical properties of the marine sediments and could be very hazardous when the sediment is unloaded in undrained conditions.
The behaviour of the unsaturated marine sediment has to be accurately identified in order to quantify the geological risks associated to the hydrate dissociation [see, for instance, Sultan, N., Cochonat, P., Foucher, J.P., Mienert, J., this volume. Effect of gas hydrates melting on seafloor slope instability]. Thus, in this work, five tests were carried out on synthetic marine sediments in order to identify the gas effect on the hydro-mechanical behaviour of unsaturated marine sediments. Based on the experimental results obtained from this study, on previous constitutive models [Alonso, E.E., Gens, A., Josa A., 1990. A constitutive model for partially saturated soils. Géotechnique 40(3), 405–430; Gens, A., Alonso, E.E., 1992. A framework for the behaviour of unsaturated expansive clays. Can. Geotech. J. 29, 1013–1032] and on the relationship of Van Genuchten [Van Genuchten, M.Th., 1980. A closed-form equation for predicting the hydraulic conductivity of unsaturated soils. Soil Sci. Soc. Am. J. 44, 892–898], a new mathematical formulation was proposed to simulate the behaviour of the unsaturated soil. Qualitative comparison between experimental results and model predictions shows the capacity of the proposed model to reasonably reproduce the essential features of the hydro-mechanical behaviour of marine unsaturated sediment. Experimental and simulation results show that unloading (tidal cycles, erosion, natural slope instabilities, excavation) a submarine unsaturated sediment slope in shallow water is much more hazardous than unloading the same submarine slope in deep water.

Keywords: unsaturated sediment; capillary pressure; triaxial tests; undrained behaviour; shear strength

1 Introduction

Temperature and/or pressure changes can modify the gas hydrate equilibrium conditions and induce gas production. Gas may alter significantly the behaviour and mechanical properties of the marine soils. For high water degrees of saturation gas bubbles are in an occluded zone within the pore fluid. For this high degree of saturation, the principle of effective stress remains valid. However, in addition to the effective stress theory, the gas compressibility (Boyle's law) and the gas solubility (Henry's law) must be considered (see for instance Atigh & Byrne 2003). For lower degrees of saturation where the gas and water phases are continuous, the effective stress theory is not valid (see for instance Coleman 1962, Matyas & Rahakrishna, 1968 and Fredlund & Morgenstern 1977) and it is essential to consider the following three state variables: 1) mean net stress (difference between mean stress and pore gas pressure) 2) the matric suction (difference between pore gas pressure and pore water pressure) and 3) deviator stress.

In marine domain, sediments with low degree of saturation (or high gas content) could be met in the vicinity of dissociating hydrate. Figure 1-a shows the in-situ measurement, using the Ifremer piezocone (Meunier et al. 2003), of the P wave velocity as a function of depth in the vicinity of gas hydrates occurrence zone. Figure 1-a shows low values of the P wave velocity measured between 10 m and 15 m below the seafloor, which correspond to sediment with low degree of saturation (around 84 % - Figure 1-b). For this type of unsaturated sediment, the Alonso et al. and Gens et al. models (Alonso et al. 1990 et Gens et al. 1992) can be accurately used to predict the hydro-mechanical behaviour. Recently several authors (Cui et al. 1995, Cui and Delage 1996, Pietruszczak and Pande 1996 among other) have used the capillary pressure as a stress state variable in order to describe the behaviour of unsaturated soil under different hydro-mechanical loadings. In general, those models have extended the Cam-clay

model for isotropic unsaturated soil. Cui et al. (1995) proposed an analytical expression of the yield curve, which allows to include the initial anisotropy of the natural soil.

The constitutive model of Alonso et al. is able to predict the volumetric strains and shear strains for any stress paths under drained conditions. However, it cannot be used to predict the behavior during undrained paths because it doesn't provide any information on the variation of degree of saturation (Wheeler 1996 and Wheeler et al. 2003). In order to take into account the behavior of unsaturated soil during sudden unloading (undrained conditions), additional equations considering the change of degree of saturation during different stress paths have to be included in the Alonso et al. model (see for instance Wheeler et al. 2003 and Sheng et al. 2004).

In this work, the unsaturated marine sediment behaviour has been first investigated in the laboratory. A new experimental apparatus was developed to control separately the different stress state variables, which characterize the behaviour of an unsaturated marine sediment. A series of experimental tests were conducted in order to identify the main features behaviour of a synthetic unsaturated soil. The obtained results were essential to the development of a new constitutive model where a special attention was devoted to the sediment behaviour under undrained conditions reproducing the behaviour at short term of marine sediment with low permeability preventing water and gas drainage.

2 Special triaxial cell for unsaturated soil

In order to examine the hydro-mechanical behaviour of unsaturated marine sediment, we have developed a new triaxial cell. This special apparatus allows distinct control of the pore-water and pore-gas pressures. The experimental device is based on the standard axis translation method in which the gas and water pressures are controlled independently allowing full control of the gas-water pressure difference. In a porous medium, the contact between two fluids induces a discontinuity of the pressure at the interface separating the two fluids. This

discontinuity of pressure is called the capillary pressure p_c. Therefore p_c is equal to the difference between the two pressures of those fluids. This capillary pressure is given by the Kelvin equation:

$$p_c = \frac{2\sigma \cos\theta}{r} \quad (1)$$

where σ is the interfacial tension between the two fluids, θ is the contact angle between the two fluids and r is the pore radius.

In order to apply a capillary pressure on the soil sample, different experimental techniques can be used. In this study, the porous plate method, also called axis translation method is used. The sample is saturated with gas and water. The method consists of bringing to bear two different pressures on both fluids using a ceramic porous stone. The main characteristic of this porous stone is its very small diameter pores, and consequently (see Equation 1) the high capillary pressure, which can be imposed between the two fluids. The disadvantage of this method is the test duration, which can be very long due to the low permeability of the porous stone.

The mechanical tests including capillary pressure control were carried out using the special triaxial cell presented in Figure 2. The soil sample (5cm of diameter, 10cm in height), contained into a membrane, is placed on a ceramic porous stone, which allows the free movement of water, but not gas, through it (in the limit of its capillary pressure). The bottom of the sample is connected to a pressure generator, which maintains the pressure of water inside the sample and control the water volume. At the top plate of the sample is applied the gas pressure. The confining pressure is imposed by a pressure generator (GDS), which allows the control of the confining pressure and the water volume surrounding the sample. In order to carry out the hydro-mechanical tests by controlling the capillary pressure, two conditions must be ensured:

- $u_g > u_w$ to prevent water passing into the gas pressure generator.
- $u_g < u_w + p_c$ to prevent gas passing through the ceramic porous stone.

The axial stress is imposed by a piston pushed down from a mechanical frame. The vertical strain is determined from the displacement of the piston (Figure 2).

3 Soil properties

In the following, the same marine sediment (silty clay) has been used for all the laboratory tests (Null Tests and hydro-mechanical test). The Atterberg limit tests carried out on the studied sediment show a liquid limit of 215% and a plastic limit of 106%, resulting in a plasticity index of 109%. The initial void ratio was around 6.2 (porosity of 0.86). The Cc coefficient (compressibility coefficient = 1), the Cs coefficient (swelling coefficient = 0.1) and the preconsolidation pressure (= 20 kPa) were determined from oedometer test carried out on saturated marine sediment. For the oedometer test and at each step loading, the consolidation coefficient and the permeability coefficient were determined. Oedometer test results are summarized in Table 2.

4 Stress state variables for unsaturated soil

Terzaghi, in 1927, defined effective stress controlling the volume changes of saturated soils, as the total mean stress minus the pore water pressure. Afterwards the concept of effective stress has been extended to other porous materials by Biot (1941), whose work formed the basis of all further developments on the coupled hydromechanical behaviour of porous materials. The extension of the effective stress concept to a porous solid containing two fluids has been tentatively made by Bishop (1959), for unsaturated soils containing water and air. Later, it was shown that this extension was unable to predict the behaviour of unsaturated soil (Jennings & Burland 1962).

Studies on the volume change behaviour of unsaturated soils showed subsequently (Coleman 1962) that the complete definition of the stress state of unsaturated soils required the definition of two stress variables : the total mean net stress σ_m-u_g and the capillary pressure $p_c = u_g$-u_w (in which σ_m is the total mean stress and u_g and u_w respectively are the gas and water pressures).

Based on experimental results, Fredlund and Morgenstern (1977) have shown that the stress state variables, governing the behaviour of an unsaturated soil, consist of two of the three possible combinations of the three isotropic tensors ($\underline{\sigma}$, $u_w\underline{1}$ and $u_g\underline{1}$):

1) $(\underline{\sigma} - u_w\underline{1})$ and $(u_g - u_w)\,\underline{1}$

2) $(\underline{\sigma} - u_g\underline{1})$ and $(u_g - u_w)\,\underline{1}$

3) $(\underline{\sigma} - u_g\underline{1})$ and $(\underline{\sigma} - u_w\underline{1})$

where $\underline{\sigma}$ is the stress tensor, u_w is the water pressure value inside the sample, u_g is the gas pressure value inside the sample and $\underline{1}$ is the tensor unit.

In their unsaturated tests, Fredlund and Morgenstern (1977) increased simultaneously the isotopic stress tensor, the water and air pressures in the sample with equal increments ($\Delta\underline{\sigma} = \Delta u_w\underline{\mathbf{1}} = \Delta u_g\underline{\mathbf{1}}$). No change of the sample and the pore water volumes were observed. They concluded that this absence of volume change was due to the constant values of the stress variables which are $\Delta(\underline{\sigma} - u_w\underline{\mathbf{1}}) = \Delta(u_g - u_w)\,\underline{\mathbf{1}} = \Delta(\underline{\sigma} - u_g\underline{\mathbf{1}}) = 0$. These tests were called *Null Tests*.

In order to validate the experimental procedures of our project, three Null Tests were carried out on the same soil sample. The summary of the stress conditions and the tests results are presented in Table 3. The sample was first saturated under a mean effective pressure of 300kPa (confining pressure equals 500kPa). The gas was then introduced into the sample at 280kPa. Once the equilibrium was reached, gas, confining water and pore water pressures were increased or decreased by the same value (see “pressure increment” column in Table 3).

Figure 3, Figure 4 and Figure 5 present the pore water volume change and the confining water volume change under an increment loading ($\Delta\sigma_3=\Delta u_w=\Delta u_g$) of 1 : +45kPa , 2 : +38kPa and 3 : -183kPa.

For the NT1 test and after 17 hours, it can be observed that only a total volume change of around 0.011 % and a water volume change of around 0.014% were observed (Figure 3). For the NT2 test, after 70 hours, the total volume change was 0.028%, and the water volume change 0.048% (Figure 4). Finally, for the NT3 test that last more than 170 hours, the maximum total volume change monitored was only 0.032%, and the maximum water volume change 0.026% (Figure 5). We can note that the sinusoidal volumes variations may be due to the temperature.

To conclude, under constant stress state variables, the total and water volume changes of the marine soil sample (Figure 3 through Figure 5) were less than 0.05%. Therefore the considered stress state variables (total mean net stress and capillary pressure) are relevant to describe the volume behaviour of an unsaturated soil.

5 Hydro-mechanical properties of unsaturated soil : experimental results

In order to identify the unsaturated sediments behaviour, five triaxial tests have been carried out on a synthetic marine soil using the cell described in paragraph 2. A fresh sample of the same marine sediment was used for each test. The shearing of the sample was obtained by an increase of the axial stress σ_1 using the mechanical piston.

The stress paths have been diversified to determine the main features of the unsaturated soil behaviour and the evolution of the shear resistance of this marine sediment with capillary pressure. Three triaxial tests were carried out at constant capillary pressure (drained conditions) and two at constant water content (undrained conditions).

5.1 Test program

The stress paths of the five triaxial tests are presented in Figure 6 in terms of the mean net stress p ($p = \sigma_m - u_g$, with σ_m the total mean stress - $\sigma_m = \frac{\sigma_1 + 2\sigma_3}{3}$ - and u_g the pore gas pressure), the capillary pressure p_c ($p_c = u_g - u_w$, with u_w the pore water pressure) and the deviatoric stress q ($q = \sigma_1 - \sigma_3$).

For each test, a sample was first water saturated (Skempton coefficient greater than 0.97) (point A in Figure 6). At the end of the saturation, the confining pressure and the pore water pressure were respectively equal to 860 kPa and 850 kPa. The sample was then isotropically consolidated (point B in Figure 6) : the total isotopic pressure was increased from 860 kPa to 1000 kPa while the bulk water pressure was maintained constant. The consolidation of the sample was verified by monitoring the bulk water volume. At the end of consolidation, the mean effective stress was equal to 150 kPa.

The **first shear test** was carried out under saturated conditions. The isotropic consolidation was followed by a drained shear test (pore water pressure remains equal to 850 kPa). The shearing rate was slow enough in order to ensure the proper drained conditions. The stress path of the first shear test corresponds to B-B' path in Figure 6. This test is a reference test for following comparisons.

For the four other tests, some carbon dioxide CO_2 was introduced in the sample (from point B to point C in Figure 6); the guest gas pressure was equal to 975 kPa. During this phase, the total mean stress σ_m and the pore water pressure were constant while the pore gas pressure was increased from 850 kPa to 975 kPa. In other words, the mean net stress decreased from 150 kPa to 25 kPa (=1000-975) and the capillary pressure increased from 0 to 125 kPa (=975-850).

The **second shear test** was carried out under the stress conditions described previously ($p = 25$ kPa and $p_c = 125$ kPa). It was a drained test. The stress path of the second shear test corresponds to C-C' path in Figure 6.

For the **third test**, from point C conditions, the soil sample was unloaded under undrained conditions (from point C to point D in Figure 6) : the total mean stress was decreased by increments from 1000 kPa to 350 kPa. Throughout the test, neither water nor gas were allowed to drain out of the sample. The pore water pressure was monitored during the unloading, while it was not possible to control the pore gas pressure. The evolution of the mean net stress p and the capillary pressure p_c were thus unknown. When the equilibrium was reached, the sample was sheared at constant water content. The third shear test corresponds to the stress path D-D' presented in Figure 6.

The behaviour of the unsaturated soil subjected to a drained decrease of the capillary pressure was tested during the **fourth test** (from point C to point E in Figure 6). The pore water pressure was increased from 850 kPa to 905 kPa, while the total mean stress and the pore gas pressure were maintained constant. In other words the mean net stress remained equal to 25 kPa and the capillary pressure was decreased from 125 kPa to 70 kPa (=975-905). When the equilibrium was reached, the sample was sheared at a constant capillary pressure. The fourth shear test corresponds to the stress path E-E' presented in Figure 6.

The **test 5** was again an unloading in undrained conditions, at the capillary pressure of 70 kPa (from point E to point F in Figure 6); the sample was then undrained sheared. This last shear test corresponds to the stress path F-F' presented in Figure 6. The five stress paths carried out within this study are summarized in Table 4.

5.2 Test results

5.2.1 Application of the gas pressure (from point B to point C in Figure 6)

For the 4 tests (2, 3, 4 and 5), the introduction of gas at a pressure of 975 kPa induced an capillary pressure increase from 0 to 125 kPa and a decrease of the mean net stress from 150 kPa to 25 kPa (see Figure 6). The volumetric strains versus time during the phase of gas introduction are presented in Figure 7.

The volume change of the unsaturated soil samples during the capillary pressure increase can be divided into 3 parts.

First, an immediate increase of the total sample volume was observed (negative volumetric strains). This expansion is due to 2 factors: on one hand the gas pressure is higher than the pore water pressure, which started up the water drainage of the sample. On the other hand, the very low permeability of the porous stone prevents the drainage process. The first initial expansion was followed by a volume decrease that corresponds to 1) the gas diffusion into the sample and 2) the water drainage. Finally, we can observe a total volume increase. Figure 7 shows that the test 2 was stopped too early. From this phase, one can see that introduction of gas into this marine sediment induces a global volume increase of the samples.

5.2.2 Decrease of the capillary pressure (from point C to point E in Figure 6)

In order to study the unsaturated soil behaviour during a capillary pressure decrease, the pore water pressure was increased from 850 kPa to 905 kPa, while mean stress and pore gas pressure remained constant (path C-E in Figure 6). In other words, the capillary pressure was decreased to 70 kPa, and the mean net stress remained equal to 25 kPa. The volume change of the samples # 4 and # 5 was monitored during the tests. For the test 5 the evolution of the volumetric strains versus time is presented in Figure 8. It can be observed that the capillary pressure decrease induces a swelling of the sample. The decrease of the capillary pressure can indeed be seen as a decrease of soil inter-particles contact forces.

5.2.3 Mechanical undrained unloading (paths E-F and C-D in Figure 6).

These tests evaluate the unsaturated soil behaviour submitted to undrained unloading at two different start capillary pressures (125 kPa for test 3 and 70 kPa for test 5). This undrained unloading simulates the unloading (tidal cycles, erosion, natural slope instabilities, excavation) of a submarine slope.

5.2.3.1 Results of the test 3

The sample was initially submitted to a 1000 kPa confining pressure, a pore water pressure of 850 kPa and a pore gas pressure of 975 kPa. The confining pressure was reduced by increments. The duration of each stage and the corresponding stress conditions are given in Table 5. Because of the experimental device, it was not possible to measure the pore gas pressure evolution during this phase. For a saturated soil, the decrease of the confining pressure in undrained conditions induces the same decrease of pore water pressure. In any case, it is not possible for the decrease of pore water pressure to be higher than the confining pressure decrease. However for the first two unloading steps, the Skempton coefficient (variation of pore water pressure Δu_w divided by variation of confining pressure $\Delta\sigma$) was greater than 1, which is probably related to the pore water dissipation generated by the previous loadings.

The last two unloading steps were probably long enough to reach the equilibrium at the end of the complete unloading. The Skempton coefficient of the complete unloading was equal to 0.87 (Table 5). From this result, we can conclude that mechanical unloading of unsaturated sediment at constant water content induces gas expansion, which generates an excess pore water pressure within the marine sediment.

5.2.3.2 Results of the test 5

For this test, the sample was initially submitted to the following stress conditions : a confining water pressure of 1000 kPa, a 905 kPa pore water pressure and a pore gas pressure of

975 kPa. The duration of each step and the corresponding stress conditions are presented in Table 6.

For this test, unloading steps were longer than the test 3. However it seems that again for the first two unloading steps, the equilibrium was not reached during the initial loading phase. The Skempton coefficient was indeed greater than 1. The evolution of pore water pressure as a function of confining pressure is presented in Figure 9.

Once equilibrium was reached (estimated at a confining pressure of 950 kPa and a pore water pressure of 782 kPa), two types of evolution of the pore water pressure can be noticed (Figure 9) :

1) For a confining pressure between 950 kPa and 700 kPa, the Skempton coefficient B (= $\Delta u_w/\Delta\sigma$) is relatively constant and equals to 0.65.
2) For a confining pressure between 700 and 350 kPa, $\Delta u_w/\Delta\sigma$ is equal to 0.35.

In Figure 10 the volumetric strains versus time for the unloading steps are presented with the confining pressure between 1000 kPa and 600 kPa. It can be observed that for the first three steps (confining pressure decreased from 1000 kPa to 900 kPa), the volumetric strains were positive (maximum volumetric strains equal 0.7%). In other words the sample volume decreases. However large negative volumetric strains (-3.5%) were observed during the decrease of the confining pressure from 900 kPa to 600 kPa (Figure 10).

During the two last unloading steps, confining pressure decreased from 600 kPa to 350 kPa and pore water pressure decreased from 582 kPa to 494 kPa. The Skempton coefficient was thus equal to 0.35. The consequence is a large expansion of the soil sample (around 4.5%) as it can be seen in Figure 11.

This test shows an important feature of the unsaturated marine sediment behaviour during unloading at constant water content:

1) The decrease of the pore water pressure is lower than the decrease of the total

confining pressure (Skempton coefficient lower than 1). Moreover the Skempton coefficient decreases with the total confining pressure.

2) The confining pressure decrease induces a gas expansion and consequently a global expansion of the marine sediment sample.

The experimental results from Figure 8 through Figure 10 show that unloading a natural submarine slope (sea level change, tidal cycles, erosion, natural slope instabilities, excavation) at low water depth is much more hazardous then unloading the same submarine slope at higher water depth.

5.2.4 Shearing

The stress conditions before shearing for the five tests are summarized in Table 7. Figure 12 presents the results of the five triaxial tests in terms of deviatoric stress, volumetric strains and shear strains.

The shear tests allow the evaluation of the gas influence on the deviatoric soil properties. The deviatoric behaviour of the 5 samples of Figure 12 can be divided into two classes. For the tests 3, 4 and 5, the deviatoric behaviour is typical of an overconsolidated soil: on one hand the deviatoric curves show a peak value following by a softening of the marine sediment. On the other hand the volumetric strain curves show an expansion of the sediment samples. For the tests 3 and 5, the soil was mechanically unloaded generating a decrease of the mean effective stress, which can explain a mechanical overconsolidated behaviour of the soil. Before shearing in test 4, the soil was submitted to a start capillary pressure of 125 kPa and it was then decreased to 70 kPa. In this case the marine sediment can be considered apparently overconsolidated (see for instance Sultan et al. 2001).

For tests 1 and 2, the soil was normally consolidated for both mechanical and hydraulic loadings. It behaves as a normally consolidated soil: a continuous hardening of the material (Figure 12-a) and a global compression of the sample during the shear test (Figure 12-b).

From the shearing tests of Figure 12-a, we can study the effect of the capillary pressure on the shear resistance of the soil. The comparison of test 1 with test 2 shows that under drained conditions, the shear resistance increases with capillary pressure (or gas content). Indeed, for an increase of 125 kPa in capillary pressure, the soil shear resistance increases by about 25 kPa (at 10% shear strain). The conclusion is that under drained conditions, an unsaturated marine soil is more resistant under shearing than a saturated soil.

Comparison of test 4 with test 5 shows a decrease of around 30 kPa of the shear resistance generated by the mechanical unloading. By comparing test 2 to test 3 a 70 kPa decrease of the shear resistance was observed. These results show that the mechanical unloading in undrained conditions generates a decrease of the marine sediment resistance. Moreover the decrease of the shear resistance depends on the initial gas content: a decrease of 30 kPa of the shear resistance at a capillary pressure of 70 kPa and a decrease of 70 kPa of the shear resistance at a capillary pressure of 125 kPa.

The conclusion of these deviatoric tests is particularly interesting in the case of shallow submarine slopes. Indeed, a sudden decrease of the total pressure (tidal cycles, erosion, excavation, small initial sediment failures) applied on a submarine unsaturated sediment slope, will generate a decrease of the sediment shear resistance below the seafloor. The decrease of the shear resistance could then initiate other important retrogressive submarine slope failures.

6 Hydro-mechanical behaviour of unsaturated soil : theoretical approach

An elastoplastic critical state framework for unsaturated soil was developed by Alonso et al. in 1990. The experimental results were quite in accordance with the model predictions for drying and loading paths. However the model was unable to reproduce the large swelling strains exhibited by certain sediments during unloading. These sediments are called expansive because of their swelling behaviour. Therefore the previous model has been modified for this type of sediment (Gens and Alonso 1992 and Alonso, Gens and Gehling 1994). The new model of Alonso, Gens and Gehling (1994) is able to predict volumetric strains and shear strains for any stress path with drained conditions. However it cannot be used to predict the behaviour during undrained paths because it doesn't provide any information on the variation of saturation degree (Wheeler 1996). Therefore, and in order to take into account this special behaviour of unsaturated soil during unloading, additional equations relating the change of degree of saturation have been included in the model of Alonso and co-workers.

Variables used for the description of the model are the stress state variables defined at section 4 : p the mean net stress ($p = \sigma_m - u_g$, with σ_m the total mean stress - $\sigma_m = \frac{\sigma_1 + 2\sigma_3}{3}$ - and u_g the pore gas pressure), the capillary pressure p_c ($p_c = u_g - u_w$, with u_w the pore water pressure) and the deviatoric stress q ($q = \sigma_1 - \sigma_3$).

6.1 Constitutive model

6.1.1 Microstructural and macrostructural behaviours

The model of Alonso et al (1994) considered two distinct levels of unsaturated soil: the microstructural level, which corresponds to the active clay minerals, and the macrostructural level, for major structure of the soil.

The microstructural level is considered saturated and the effective stress concept may be used. The microstructural strains are considered volumetric and elastic, and independent of the macrostructure; these strains depend only on the increment $d(p + p_c)$. Therefore, the straight line $p + p_c = constant$ is a neutral line, where no microstructural deformations occur. This line is called Neutral Line (NL, see Figure 13), and separates the zone of microstructural swelling and the zone of microstructural collapse in the p-p_c plane.

Two additional yield loci are introduced in the model : Suction Increase (SI) line and Suction Decrease (SD) line (see Figure 13). They are parallel to the Neutral Line NL and define the elastic area, in which strains are only reversible. Irreversible strains are generated when the stress state reaches one of these two lines.

The yield locus related at the macrostructural level is the LC surface (see Figure 13). When the stress path crosses this yield curve in the p-p_c plane, irreversible macrostructural volumetric strains occur. This may be due to a decrease of capillary pressure (which induces collapse strains), or an increase of loading (which induces loading strains). To the left of this curve, in the elastic area, a change of p or p_c induces reversible strains.

A coupling exists between these three yield surfaces SD, SI and LC. Lets consider a soil sample, that is affected by a decrease of capillary pressure (from point A to point B in Figure 14-a). This decrease of p_c induces the development of microstructural swelling (SD_i tends towards SD_f). Thus, the soil skeleton (macrostructure) will be affected by this swelling, and the macrostructural void ratio increases. This plastic volume change leads in turn to a movement of the yield surface LC to the left (LC_i tends towards LC_f). The microstructural level is affected by the swelling, and yield curve SI moves too (SI_i tends towards SI_f).

Figure 14-b presents the coupling due to an increase of the capillary pressure p_c.

These coupling are expressed by the hardening laws.

For triaxial stress state, the deviatoric stress variables q is used. The developed model is based on the modified Cam Clay model. Thus, in the p-q plane, the yield curve for a sample at constant capillary pressure p_c is described by an ellipse (see Figure 15). Yield lines SI and SD extend into the region q>0 by means of planes parallel to the q axis (see Figure 15).

6.1.2 Mathematical formulation

6.1.2.1 Elastic behaviour

For stress paths inside the elastic area, Alonso et al.(1990) suggested the following equation for volumetric elastic strains:

$$d\varepsilon_{vM}^{e} = \frac{\kappa}{v}\frac{dp}{p} + \frac{\kappa_s}{v}\frac{dp_c}{p_c + p_{at}} \tag{2}$$

where v is the specific volume, κ and κ_s are respectively the elastic stiffness parameters for changes in p and p_c, and p_{at} is atmospheric pressure.

For triaxial stress states, a change in deviatoric stress generates shear elastic strains given by :

$$d\varepsilon_{s}^{e} = \frac{dq}{3G} \tag{3}$$

The microstructural volumetric strain $d\varepsilon_{vm}^{e}$ associated with changes in $\left(p + p_c\right)$ is expressed by :

$$d\varepsilon_{vm}^{e} = \beta_m \exp\left(-\alpha_m\left(p + p_c\right)\right) d\left(p + p_c\right) \tag{4}$$

where β_m and α_m are microstructural parameters.

6.1.2.2 Yield curves

The preconsolidation pressure p_0, for the considered capillary pressure p_c, defines the position of the LC yield surface in the p-p_c plane; it is expressed through the following

relation :

$$\frac{p_0}{p_r} = \left(\frac{p_{c0}}{p_r} \right)^{\frac{\lambda(0)-\kappa}{\lambda(p_c)-\kappa}} \tag{5}$$

where p_{c0} is the preconsolidation stress for saturated conditions, p_r is a reference stress, $\lambda(0)$ is the slope of the virgin saturated consolidation line and $\lambda(p_c)$ is a stiffness parameter given by :

$$\lambda(p_c) = \lambda(0)\left[(1-r)\exp(-\beta p_c) + r \right] \tag{6}$$

where r is a parameter defining the maximum soil stiffness and β is a parameter controlling the rate of increase of soil stiffness with capillary pressure.

$\lambda(p_c)$ corresponds to the slope of the virgin consolidation line at capillary pressure p_c.

In the p-q plane, the yield curve is an ellipse, which extends due to capillary pressure increase; its equation is:

$$q^2 - M^2\left(p + kp_c \right)\left(p_0 - p \right) = 0 \tag{7}$$

where M is the slope of critical state lines and k is a parameter describing the cohesion increase with capillary pressure.

In the model of Cam Clay, the failure state is defined by a critical state line in the p-q plane; this line goes through origin with the slope M (see Figure 16). The effect of capillary pressure on the sample is to increase the cohesion; this feature can be represented in terms of the critical state line by maintaining the slope M and by intersecting the p axis at the point at which $p = -p_s = -kp_c$. (Figure 16).

6.1.2.3 Flow rules

Microstructural strains $d\varepsilon_{vm}^{e}$ lead to softening/hardening of the macrostructure by the development of irreversible strains $d\varepsilon_{vM}^{p}$ when yield curves are reached.

When yield curve SI or SD is reached, a change in p or p_c leads to the following plastic strains, respectively $d\varepsilon_{vMI}^{p}$, $d\varepsilon_{vMD}^{p}$:

$$d\varepsilon_{vMI}^{p} = \beta_m \exp(-\alpha_m (p + p_c))\, d(p + p_c)\, t_I \left(1 - \frac{p}{p_0}\right)^{n_I} \tag{8}$$

$$d\varepsilon_{vMD}^{p} = \beta_m \exp(-\alpha_m (p + p_c))\, d(p + p_c)\, t_D \left(1 - \frac{p}{p_0}\right)^{n_D} \tag{9}$$

where p is the current mean net stress, p_0 is the preconsolidation stress for the considered capillary pressure and t_I, t_D, n_I and n_D are model parameters.

Once the LC surface is reached an increase of the total mean net stress or/and the capillary pressure induces plastic irreversible strains $d\varepsilon_v^p$. In case of triaxial stress, the plastic shear strain increment $d\varepsilon_q^p$ depends on the plastic volumetric strain increment $d\varepsilon_v^p$ with the relation:

$$\frac{d\varepsilon_q^p}{d\varepsilon_v^p} = \frac{2\alpha q}{M^2 (2p + kp_c - p_0)} \tag{10}$$

The constant α is equal to :

$$\alpha = \frac{M(M-9)(M-3)}{9(6-M)} \left\{ \frac{1}{1 - \kappa/\lambda(0)} \right\} \tag{11}$$

6.1.2.4 Hardening laws

Positions of SD and SI are defined with parameters s_h and s_0 respectively (see Figure 15).

SI and SD hardening is governed by the total volumetric plastic strain due to activation of SI

and SD ($d\varepsilon_{vMI}^{p} + d\varepsilon_{vMD}^{p}$). The hardening law for the yield locus SI is expressed by:

$$ds_0 = \frac{d\varepsilon_{vMI}^{p} + d\varepsilon_{vMD}^{p}}{\beta_m \, e^{-\alpha_m s_0} \, t_I \, (1 - p / p_0)^{n_I}} \tag{12}$$

Similary, for the yield locus SD:

$$ds_h = \frac{d\varepsilon_{vMI}^{p} + d\varepsilon_{vMD}^{p}}{\beta_m \, e^{-\alpha_m s_h} \, t_D \, (1 - p / p_0)^{n_D}} \tag{13}$$

Once the LC surface is reached, the plastic strains generate an increase of the preconsolidation pressure previously reached by the soil. In the model, it is postulated that microstructure has influence on macrostructure; so the hardening law of LC is given by Equation 14 where p_{c0} depends on the microstructural plastic strains $d\varepsilon_{vM}^{p}$:

$$\frac{dp_{c0}}{p_{c0}} = \frac{v}{\lambda(0) - \kappa} (d\varepsilon_{v}^{p} + d\varepsilon_{vMI}^{p} + d\varepsilon_{vMD}^{p}) \tag{14}$$

6.2 Hydro-mechanical behaviour of unsaturated soil under constant water content

The model previously described can not predict tests at constant water content because there are no relations between water content (or water degree of saturation Sr_w) and the three stress state variables (p,q,p_c).

Alonso et al (1990) proposed a relationship where the degree of saturation Sr_w depends markedly on capillary pressure p_c whereas the influence of applied stress is small :

$$Sr_w = 1 - L \tanh(Np_c) \tag{15}$$

where L and N are constants. This relation can be used for water degree of saturation greater than 0.4.

An other relationship, between Sr_w and p_c, has been proposed by Van Genuchten (1980) for the whole range of degree of saturation:

$$p_c = u_g - u_w = \frac{\left[\left(\frac{Sr_w - \theta_r}{\theta_s - \theta_r}\right)^{\frac{-1}{m}} - 1\right]^{\frac{1}{n}}}{\alpha} \tag{16}$$

This relation needs the knowledge of five shape parameters: θ_r , θ_s , α , m and n (Figure 17). In this work, in order to consider the whole range of degree of saturation, we use the relation proposed by Van Genuchten.

6.2.1 Compressibility and solubility of the gas

Experimental results have shown that the decrease of pore water pressure during unsaturated soils undrained unloading is smaller than the decrease of total stress. This particular behaviour is due to the gas compressibility and solubility.

The compressibility of a free gas is described by Boyle's law which states that the gas volume varies inversely with gas pressure at a constant temperature. The gas solubility is described by Henry's law which states that the mass of gas dissolved in the water is directly proportional to the absolute gas pressure above the solution, at a constant temperature.

6.2.2 Model formulation

By differentiating Equation 16 with respect to time, we obtain:

$$du_g - du_w = \frac{-\left[\left(\frac{Sr_w - \theta_r}{\theta_s - \theta_r}\right)^{-\frac{1}{m}} - 1\right]^{\frac{1}{n}}}{n} \frac{\left(\frac{Sr_w - \theta_r}{\theta_s - \theta_r}\right)^{-\frac{1}{m}}}{\left[m\left(Sr_w - \theta_r\right)\left[\left(\frac{Sr_w - \theta_r}{\theta_s - \theta_r}\right)^{-\frac{1}{m}} - 1\right]\alpha\right]} dSr_w \qquad (17)$$

where du_g and du_w are respectively gas and water pore pressure increments, and dSr_w is the degree of saturation increment.

In this equation, the effect of the changes in porosity (and thus in m, n, α, θ_s and θ_r) is neglected with regard to the evolution of Sr_w.

The volumetric strain rate $d\varepsilon = -dV_v/V$ (where V_v is voids volume and V total volume) can be expressed in terms of $d\varepsilon^g = -dV_g/V$ and $d\varepsilon^w = -dV_w/V$ (where dV_g and dV_w are respectively gas and water volume change), then :

$$d\varepsilon = \frac{V_g}{V} d\varepsilon^g + \frac{V_w}{V} d\varepsilon^w \qquad (18)$$

Considering water to be incompressible, we have $dV_w = 0$. Thus, since $Sr_w = V_w / V_v$, and using Equation 18, we find:

$$dSr_w = Sr_w\left(1 - Sr_w\right) d\varepsilon^g \qquad (19)$$

Equation 18 can be supplemented by the constitutive relation between variation of gas volume and variation of gas pore pressure:

$$du_g = K_a \, d\varepsilon^g \qquad (20)$$

where K_a is the bulk modulus of air. Using Boyle's and Henry's laws to the total volume of

gas (free gas V_g and dissolved gas V_d), the modulus K_a is developed, and we obtain the following relation:

$$du_g = (u_g + p_{at}) \left(\frac{1 - Sr_w}{1 - Sr_w + HSr_w} \right) d\varepsilon^g \tag{21}$$

where H is the coefficient of solubility. Although the value of H is affected by the gas pressure (H increases with increasing gas pressure), it is taken constant in the model.

The change of gas and water pore pressures due to change of total stress at constant water content cannot be directly determined with the previous equations. For each increment of total stress, the change of gas pore pressure is first arbitrarily chosen; the change of gas volume is calculated with Equation 21, as well as changes of degree of saturation and water pore pressure (with equations 17 and 19). Therefore, the new stress paths are completely determined and the total volume change of the soil is calculated using the Alonso et al. (1990) model. The correct gas pressure value is then calculated by iteration in order to obtain a soil volume change from the Alonso et al. model equal to the gas volume change obtained from equation 21.

6.3 Model parameters

The parameters used in the model previously described are: parameters of initial state (p_{c0}, s_0, s_h, e_0, S_{r0}); parameters associated with LC yield curve ($\lambda(0)$, κ, β, p_c, r); parameters associated with capillary pressure changes (κ_s, α_m, β_m, t_I, n_I, t_D, n_D); and parameters associated with changes in shear stress and strength (G, M, k).

The determination of the model parameters requires capillary pressure-controlled tests. Isotropic drained compression tests at several constant capillary pressure values provide data to determine parameters associated with LC yield curve ($\lambda(0)$, κ, β, p_c, r) and the

preconsolidation stress for saturated conditions p_{c0}. In the same way, drying-wetting cycles at constant mean net stress values allow to obtain κ_s, s_0 and s_h; with the same tests α_m, β_m, t_I, n_I, t_D, n_D may be approximated with percentage of irreversible strains. Parameters G, M, k are obtained with drained shear strength tests at different capillary pressures. The five parameters (θ_r, θ_s, α, m, n) of the equation of Van Genuchten (Equation 16) are determined from the mercury porosimeter curve.

6.4 Model predictions

Due to the lack of experimental data for marine unsaturated sediment, allowing the determination of the relevant parameters, and in order to validate the implementation of the proposed model, we consider a theoretical case where the unsaturated sediment is taken at 40 m below the seafloor, with a total sediment unit weight of 16 kN/m^3. The gas is the carbon dioxide. The parameters used for the theoretical simulations are indicated in Table 8. The Henry's constant is taken to be equal to 0.00027; the drainage curve parameters (θ_r, θ_s, α, m, n) are taken respectively as 0.083, 1.09, 0.0167 kPa^{-1}, 99% and 5%.

6.4.1 Volumetric behaviour of unsaturated soil: unloading under undrained conditions

In the following, we simulate the response of the marine soil (with the parameters described in Table 8) for different stress paths under undrained conditions using the model previously described.

For unloading, and as a case study, we consider the response of the soil under 3 undrained unloading stages which correspond respectively to the loss of 2 m (point 1 - Figure 18), 6 m (point 2 - Figure 18) and 10 m (point 3 - Figure 18) of the soil layer thickness (tidal cycles, erosion, excavation or slope instability) above the considered marine sediment sample.

Figure 18-a presents the gas pressure evolution during the undrained unloading generated by

the soil layer thickness decreases above the considered marine sediment. This curve shows a non-linear decrease of gas pressure with the mean stress decrease. Above 550 kPa, the unloading stress path is in the elastic area, and a small gas pressure decrease is observed (only 2 kPa) for a decrease of 100 kPa of the mean stress. When the stress path reaches the SD yield surface (point 2), the volumetric strain of the soil (which is equal to the change of volume of gas) becomes more important, and so the gas pressure decreases more quickly ($\Delta u_g/\Delta\sigma = 0.1$). In Figure 18-b the capillary pressure as a function of the mean stress during the unloading process is presented. One can observe an increase of the capillary pressure generated by a decrease of the total stress. The very small increase calculated here is a consequence of the used parameters.

6.4.2 Deviatoric behaviour of unsaturated soil : unloading under undrained conditions

In terms of deviatoric behaviour, the undrained unloading has no consequence for saturated soil. However, for unsaturated marine sediment the decrease of the mean net stress induces a decrease of the shear strength. In Figure 19 we present the shear strength as a function of shear strains for the three unloaded cases in Figure 18. Figure 19 shows clearly a decrease of the maximum shear strength with the increase of the unloading level. For unloading corresponding to 10 m of the soil thickness above the considered marine sediment sample, one can observe a drop of around 60 % of the maximum shear strength with respect to the intact soil layer. From Figure 19, one can conclude that the shear strength of unsaturated marine sediment is strongly influenced by the total stress levels under undrained conditions. Figure 19 shows clearly that unsaturated marine sediment behaviour could be very hazardous when it is unloaded in undrained conditions. The simulation results show that unloading a natural submarine slope (tidal cycles, erosion, natural slope instabilities, excavation) at low water depth is much more hazardous then unloading the same submarine slope at higher water depth.

7 Conclusions

In our project, a new triaxial cell was developed in order to control separately the different stress state variables, controlling the marine unsaturated sediment behaviour. Three null tests were carried out to identify the stress state variables. A series of experimental tests were conducted to identify the main behaviour of a synthetic unsaturated marine sediment. Special attention was devoted to the experimental behaviour of the unsaturated marine sediment under undrained conditions, which simulates the sudden unloading (tidal cycles, erosion, natural slope instabilities, excavation) of a submarine slope. The experimental results have shown that a decrease of the capillary pressure under undrained conditions (so an increase of the degree of saturation) generates a swelling of the soil.

The increase of the capillary pressure (decrease of the degree of saturation) in drained conditions increases the shear resistance of the marine sediment. However, the mechanical undrained unloading generates on one hand a decrease of the mean effective stress and on the other hand an important decrease of the undrained shear sediment resistance. Thus, unloading in undrained conditions an unsaturated marine sediment could be very hazardous.

The development of a new mathematical formulation based on previous constitutive models (Alonso et al. 1990 and Gens et al. 1992), allowed the prediction of the main features of unsaturated marine sediment behaviour.

Simulation results in terms of volumetric behaviour show that during undrained unloading, the Skempton coefficient decreases with the total load. For the deviatoric behaviour, the undrained unloading induces a decrease of the undrained shear strength , which depends on the total stress levels. Qualitative comparison between experimental results and model predictions shows the capacity of the proposed model to reproduce reasonably the essential features of the hydro-mechanical behaviour of unsaturated marine soil. Experimental and simulations results show that unloading (tidal cycles, erosion, natural slope instabilities,

excavation) a submarine unsaturated sediment slope at low water depth is much more hazardous then unloading the same submarine slope at higher water depth.

REFERENCES

Alonso E.E., Gens A., Josa A., 1990. A constitutive model for partially saturated soils. Géotechnique 40(3), 405-430.

Alonso E.E., Gens A., Gehling W.Y, 1994. Elastoplastic model for unsaturated expansive soils. In: Smith (ed.), Numerical Methods in Geotechnical Engineering.

Alonso E.E., Vaunat J., Gens A., 1999. Modelling the mechanical behaviour of expansive clay. Engineering Geology 54, 173-183.

Biot M.A., 1941. General theory of three-dimensional consolidation. Journal of Applied Physics 12, 155-164.

Bishop A.W., 1959. The principle of effective stress. Tecknisk Ukeblad 106(39), 859-863.

Coleman J.D., 1962. Stress strain relations for partly saturated soil. Géotechnique 12(4), 348-350.

Cui, Y.J., Delage, P. and Sultan, N., 1995. An Elastoplastic Model for Compacted Soils, Unsaturated Soils/ Proc. 1st Int. Conf. on Unsaturated Soils (UNSAT 95), Alonso, E.E. and Delage, P. (Eds), Rotterdam,pp. 703-709.

Cui, Y.J. and Delage, P., 1996. Yielding and plastic behaviour of an unsaturated compacted silt. Géotechnique 46: 291-311.

Fredlund D.G. & Morgenstern N.R., 1977. Stress state variables for unsaturated soils. ASCE 103(GT5), 447-466.

Gens A., Alonso E.E., 1992. A framework for the behaviour of unsaturated expansive clays. Canadian Geotechnical Journal 29, 1013-1032.

Jennings J.E.B. & Burland J.B., 1962. Limitations to the use of effective stresses in partly saturated soils. Géotechnique 12(2), 125-144.

Matyas, E.L. and Radhakrishna, H.S. 1968. Volume change characteristics of partially saturated soil. Géotechnique 18, 432-448.

Meunier, J., Sultan, N., Jegou, P and Harmegnies F. 2004. First tests of Penfeld: a new seabed penetrometer. Proceedings of The Fourteenth International Offshore and Polar Engineering Conference, Toulon, France.

Pietruszczak, S. and Pande, G.N., 1996. Constitutive relations for partially saturated soils containing gas inclusions. Journal of Geotechnical Engineering 122 (1), 50-59.

Sheng, D., Sloan S.W. and Gens A. 2004. A constitutive model for unsaturated soils: thermomechanical and computational aspects. Computational Mechanics, 33.

Sultan N., Cochonat P., Dennielou B., Bourillet J.F., Savoye B. and Colliat J.L. 2000. Surconsolidation apparente et pression osmotique dans un sédiment marin, Comptes Rendus de l'Académie des Sciences - Series IIA - Earth and Planetary Science, 331(5),379-386.

Sultan N., Cochonat P., Foucher J.P. and Mienert J. this volume. Effect of gas hydrates melting on seafloor slope instability.

Terzaghi, C., 1927. Principles of Final Soil Classification. Public Roads 8(3), 41-53.

Van Genuchten, M. Th., 1980. A closed-form equation for predicting the hydraulic conductivity of unsaturated soils. Soil Science Society Am. Journal 44, 892-898.

Wheeler S.J., 1988. A conceptual model for soils containing large gas bubbles. Géotechnique 38, 389-397.

Wheeler S.J., 1996. Inclusion of specific water volume within an elasto-plastic model for unsaturated soil. Canadian Geotechnical Journal 33, 42-57.

Wheeler S.J., Sharma R.S. and Buisson MSR, 2003. Coupling of hydraulic hysteresis and stress-strain behaviour in unsaturated soils. Geotechnique 53(1), 41–54.

Void ratio e(-)	Permeability k ($m.s^{-1}$)	Consolidation coefficient Cv (m^2/s)	Loading (kPa)
5.72	$2.495*10^{-9}$	$2.66*10^{-8}$	25
5.26	$1.457*10^{-9}$	$1.26*10^{-8}$	51
4.40	$6.29*10^{-10}$	$9.429*10^{-9}$	102
3.76	$3.22*10^{-10}$	$9.5*10^{-9}$	204

Table 2 : Sample properties

Test Number	Pressure increment (kPa)	Consolidation pressure			Maximum sample volume change (%)	Maximum water volume change (%)
		Total (kPa)	Gas (kPa)	Water (kPa)		
NT1	+ 45	545	325	245	- 0.011	+ 0.014
NT2	+ 38	583	363	283	- 0.028	+ 0.048
NT3	- 183	453	210	153	- 0.032	+ 0.026

Table 3 : Summary of the Null Tests.

	Stress path	Shearing Conditions		
			p	p_c
Test 1	Saturation – consolidation - shearing	drained	150 kPa	0 kPa
Test 2	Saturation – consolidation – gas introduction – shearing	drained	25 kPa	125 kPa
Test 3	Saturation – consolidation – gas introduction – undrained unloading - shearing	undrained	unknown	unknown
Test 4	Saturation – consolidation – gas introduction – capillary pressure decreasing - shearing	drained	25 kPa	70 kPa
Test 5	Saturation – consolidation – gas introduction – capillary pressure decreasing – undrained unloading - shearing	undrained	unknown	Unknown

Table 4 : Characteristics of the experimental tests performed

Number of step	Applied confining pressure (kPa)	Measured pore water pressure (kPa)	Skempton Coefficient	Duration of the step (minute)
Initial state	1000	850		
1	900	737	1.13*	306
2	700	516	1.11*	1110
3	500	374	0.71	1464
4	350	283	0.607	7183
Total			**0.87**	

* equilibrium was not reached during the initial loading phase

Table 5: Phase of unloading at constant water content for test 3 (from C to D in Figure 6).

Number of step	Confining pressure (kPa)	Pore water pressure (kPa)	Skempton coefficient	Duration of the step (minute)
Initial state	1000	890		40
1	970	814	2.53*	1509
2	950	782	1.60*	1649
3	900	747	0.70	1460
4	800	695	0.52	1290
5	700	621	0.74	2674
6	600	582	0.39	1895
7	500	553	0.29	1400
8	350	494	0.39	6830
Total			**0.61**	

* equilibrium was not reached during the initial loading phase

Table 6 : Step of unloading at constant water content for test 5 (from E to F in Figure 6).

Test Number	Confining pressure (kPa)	Pore water pressure (kPa)	Pore gas pressure (kPa)	Mean net stress (kPa)	Capillary pressure (kPa)	Drained/ undrained
1	1000	850	850	150	0	Drained
2	1000	850	975	25	125	Drained
3	350	283	unknown	unknown	unknown	Undrained
4	1000	905	975	25	70	Drained
5	350	494	unknown	unknown	unknown	Undrained

Table 7 : Stress conditions before shearing for the five tests.

Parameters associated with												
LC yield surface					Capillary pressure changes					Shear		
$\lambda(0)$	K	β	p_c	R	κ_s	α_m	β_m	n	t	G	M	k
		kPa^{-1}	kPa			kPa	kPa^{-1}			kPa		
0.22	0.022	$1*10^{-4}$	5	0.55	$9*10^{-4}$	$6*10^{-5}$	$1.4*10^{-5}$	0.01	10	5000	1.4	0.8

Table 8 : Model parameters

LIST OF FIGURES

Figure 1: a) In-situ measurement of the P wave velocity as a function of depth b) gas degree of saturation (Sg) calculated from the P wave velocity profile using the effective medium theory (Helgerud et al. 1999).

Figure 2: Triaxial cell for unsaturated soil

Figure 3: Result from NT1 Test

Figure 4: Result from NT2 Test

Figure 5: Result from NT3 Test

Figure 6: Stress paths for the five experimental tests

Figure 7. Volumetric strains - time diagram during application of the gas pressure (path B-C in Figure 6)

Figure 8: Volumetric strains during capillary pressure decreasing for test 5 (path C-E in Figure 6)

Figure 9: Evolution of pore water pressure as a function of the confining pressure during unloading at constant water content (test 5, from E to F in Figure 6)

Figure 10: Volumetric strains and confining pressure versus time for different unloading steps at constant water content

Figure 11: Volumetric strains and confining pressure versus time generated by a decrease of the confining pressure from 600kPa to 350kPa at constant water content

Figure 12: a) Deviatoric stress - shear strains diagram b) Volumetric strains - shear strains diagram

Figure 13: Yield loci in $p\text{-}p_c$ plane

Figure 14: Coupling between microstructural and macrostructural yield curves a) With a decrease of capillary pressure – b) With an increase of capillary pressure

Figure 15: Yield surfaces in $p\text{-}q\text{-}p_c$ space -a) Cross section in $p\text{-}p_c$ plane -b) Cross section in p-q plane

Figure 16: Position of the Critical State Line (CSL) in the p-q plane

Figure 17: Parameters used in the Van Genuchten equation (Equation 16)

Figure 18: a) Gas pressure - mean net stress relationship b) Capillary pressure - mean net stress relationship for unsaturated soil

Figure 19: Shear stress-shear strains relationships under undrained conditions for an unsaturated soil

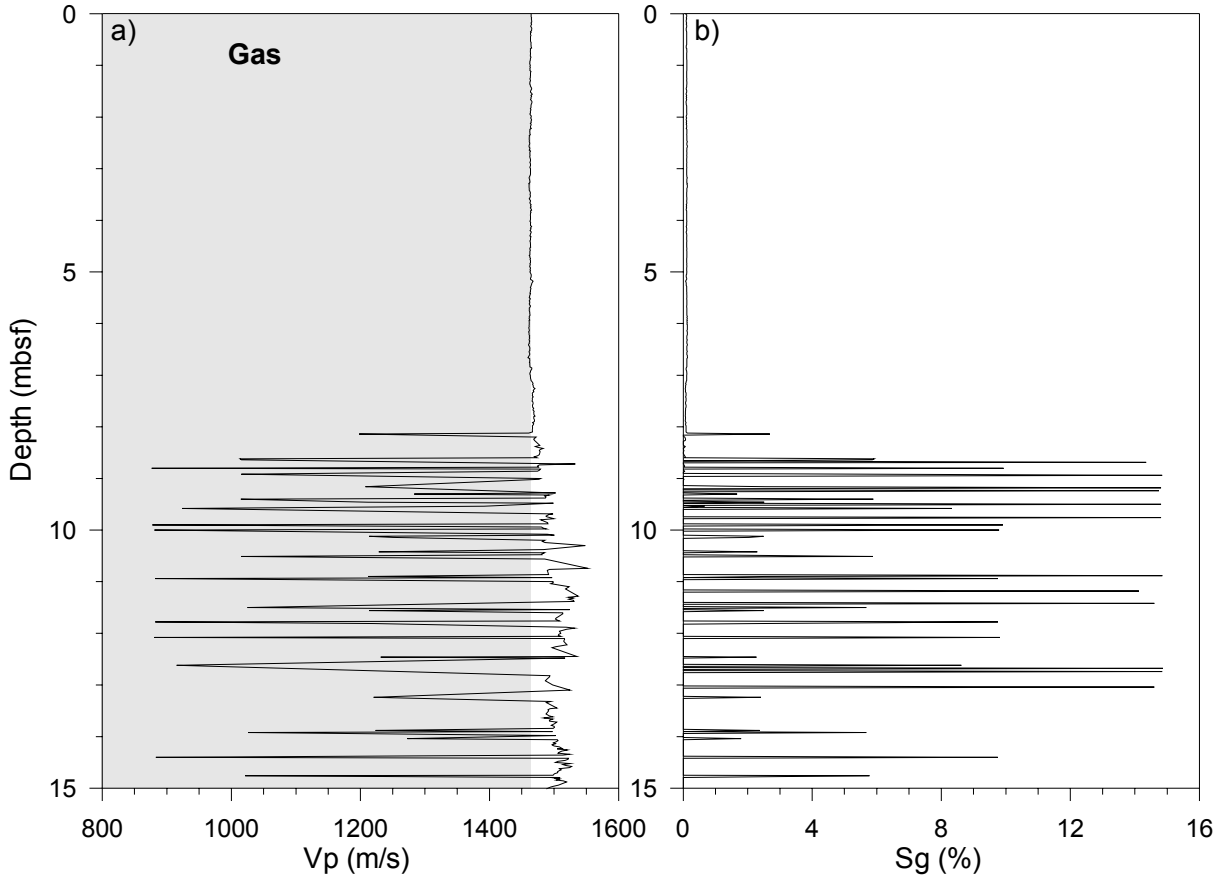

Figure 1: a) In-situ measurement of the P wave velocity as a function of depth b) gas degree of saturation (Sg) calculated from the P wave velocity profile using the effective medium theory (Helgerud et al. 1999).

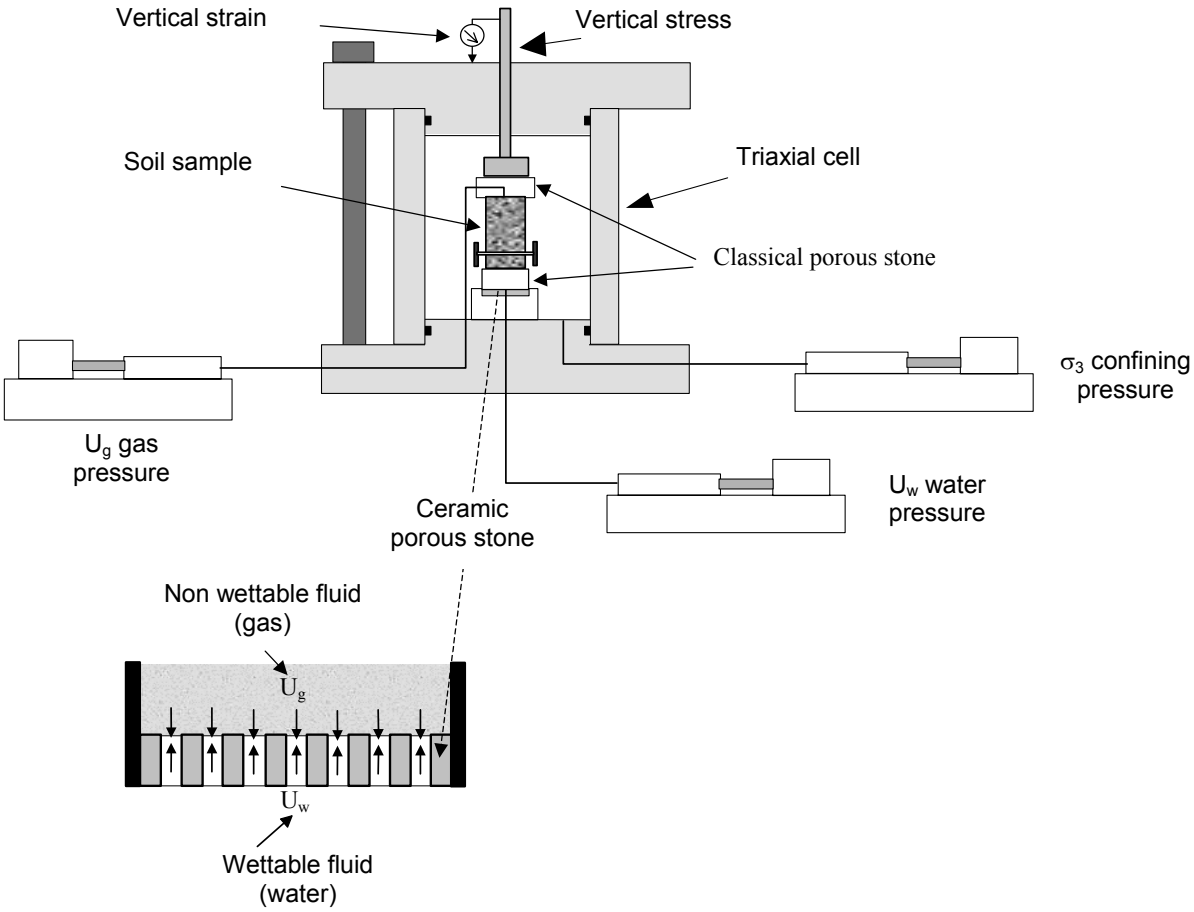

Figure 2: Triaxial cell for unsaturated soil

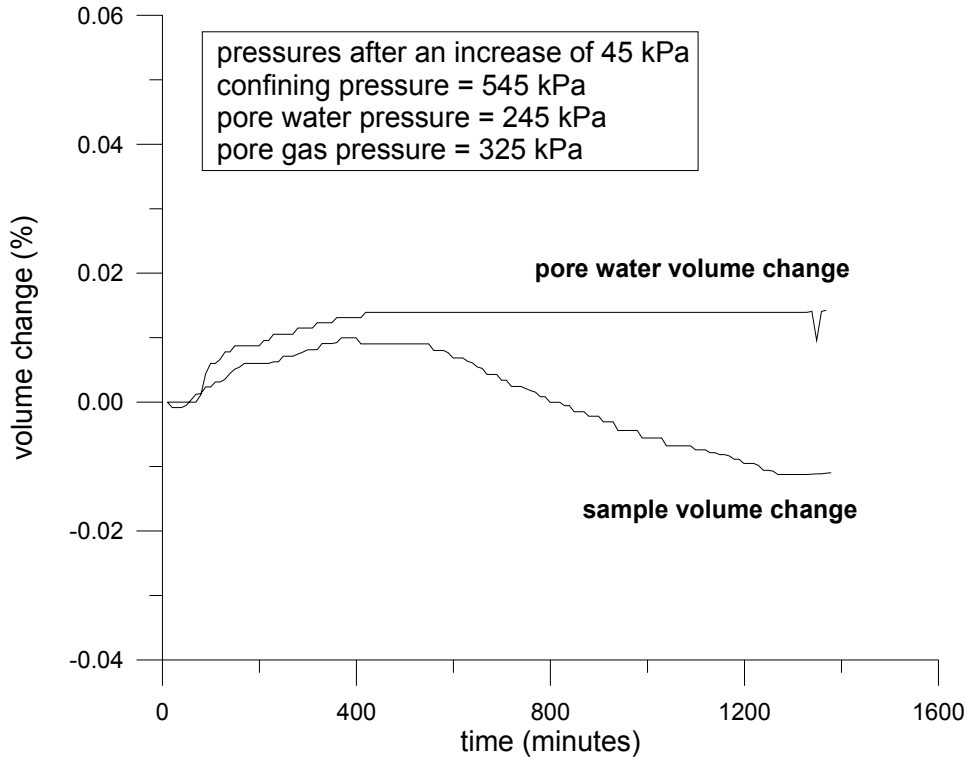

Figure 3: Result from NT1 Test

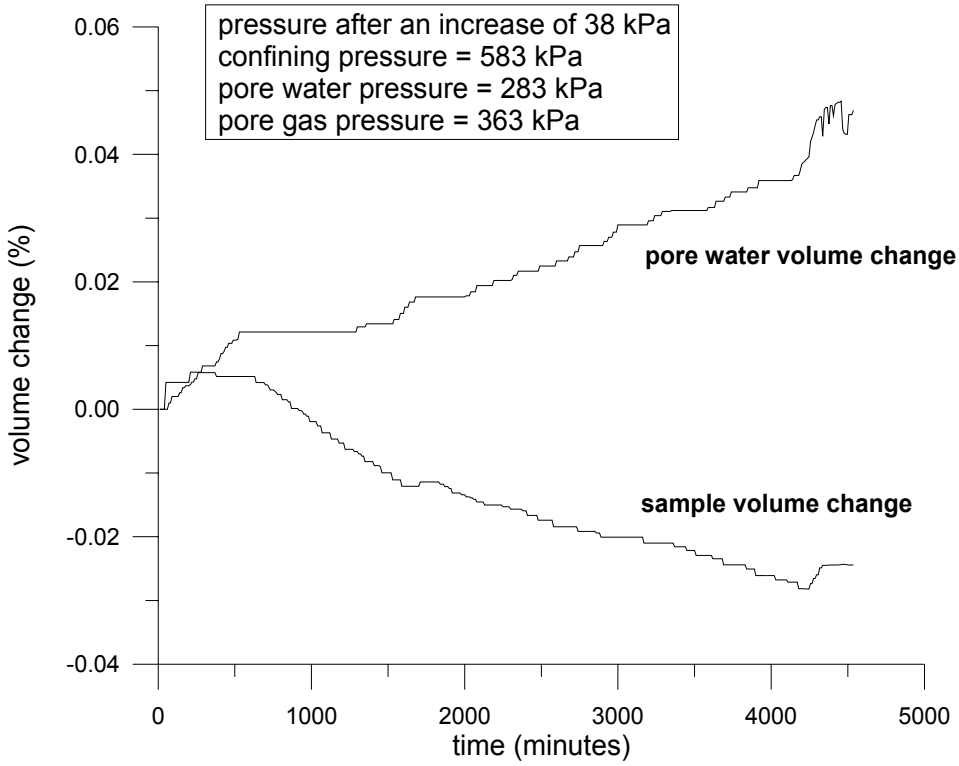

Figure 4: Result from NT2 Test

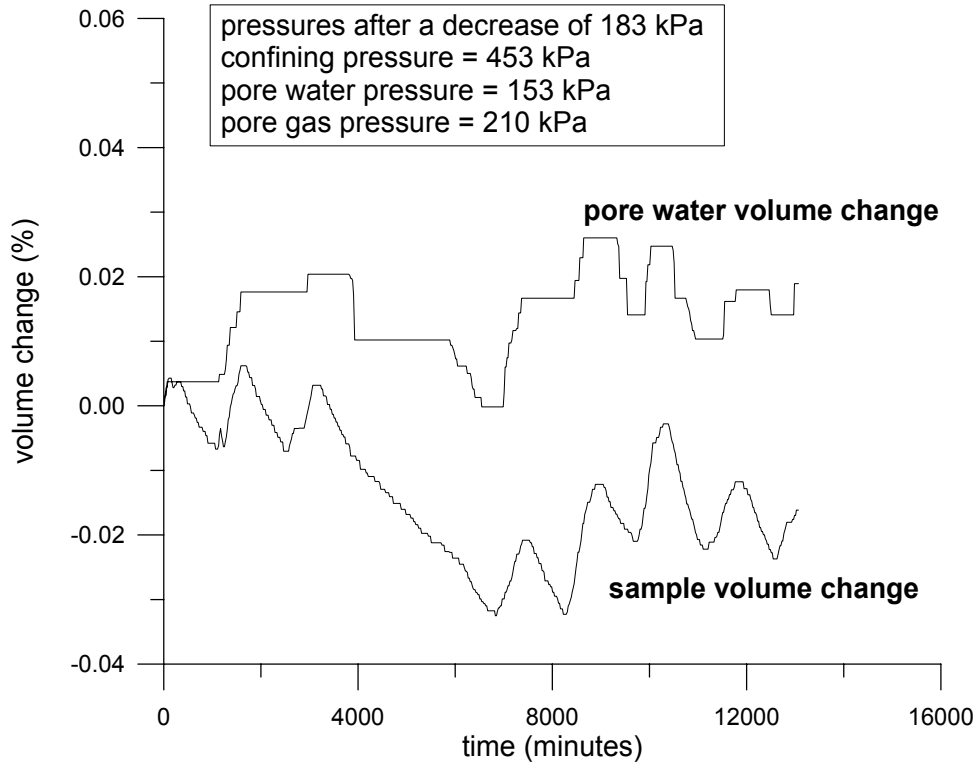

Figure 5: Result from NT3 Test

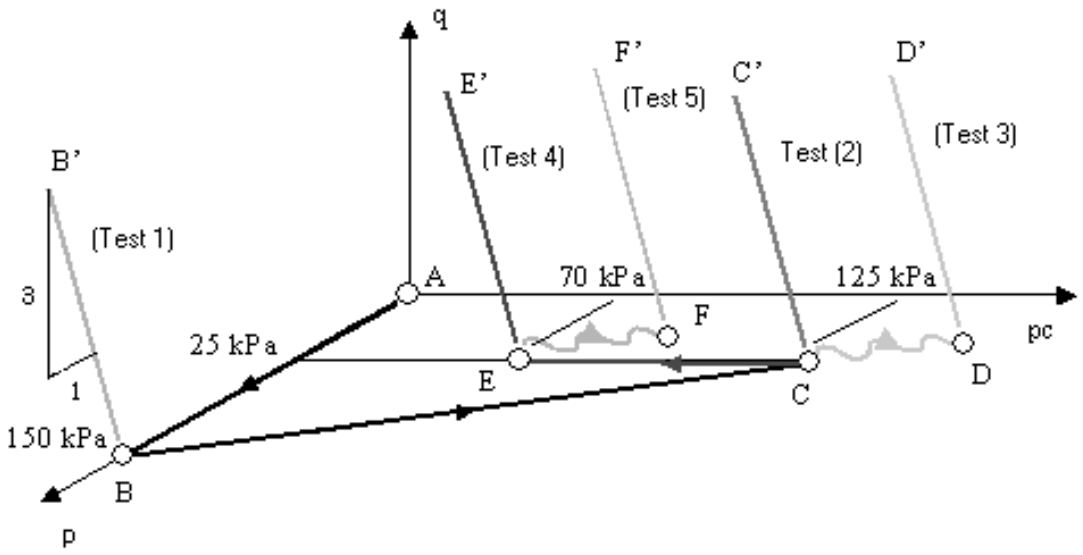

Figure 6: Stress paths for the five experimental tests

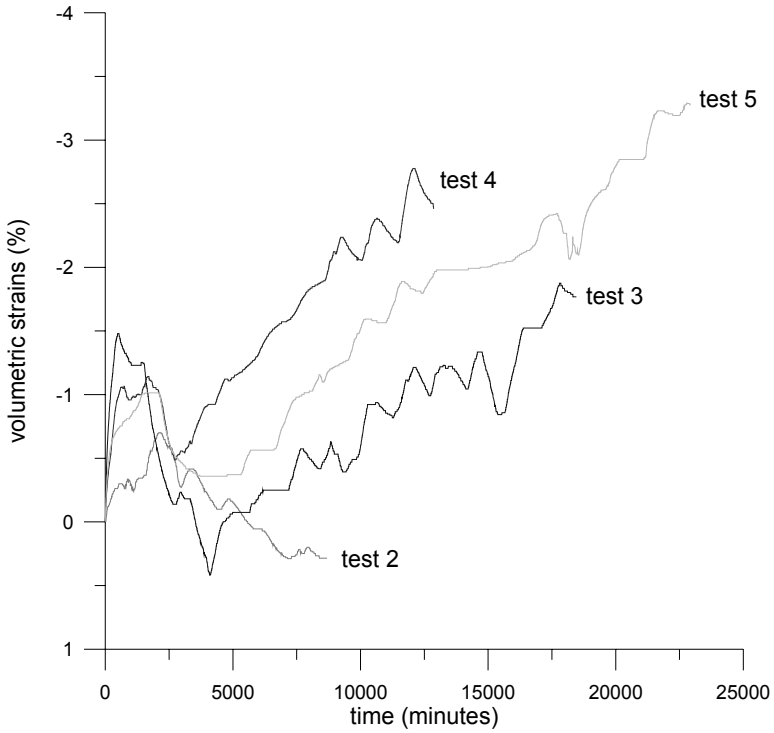

Figure 7. Volumetric strains - time diagram during application of the gas pressure (path B-C in Figure 6)

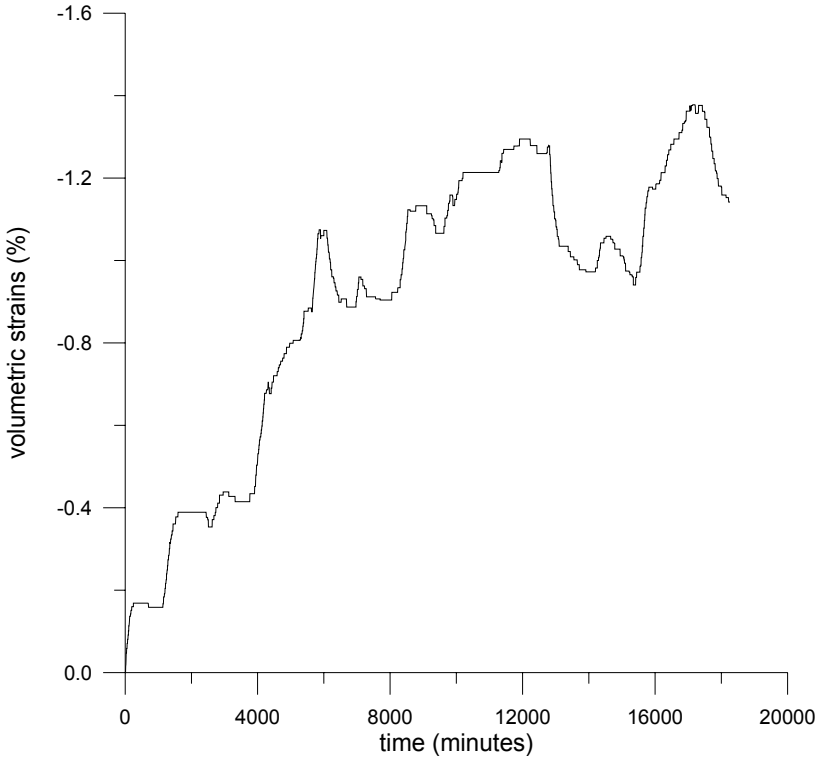

Figure 8: Volumetric strains during capillary pressure decreasing for test 5 (path C-E in Figure 6)

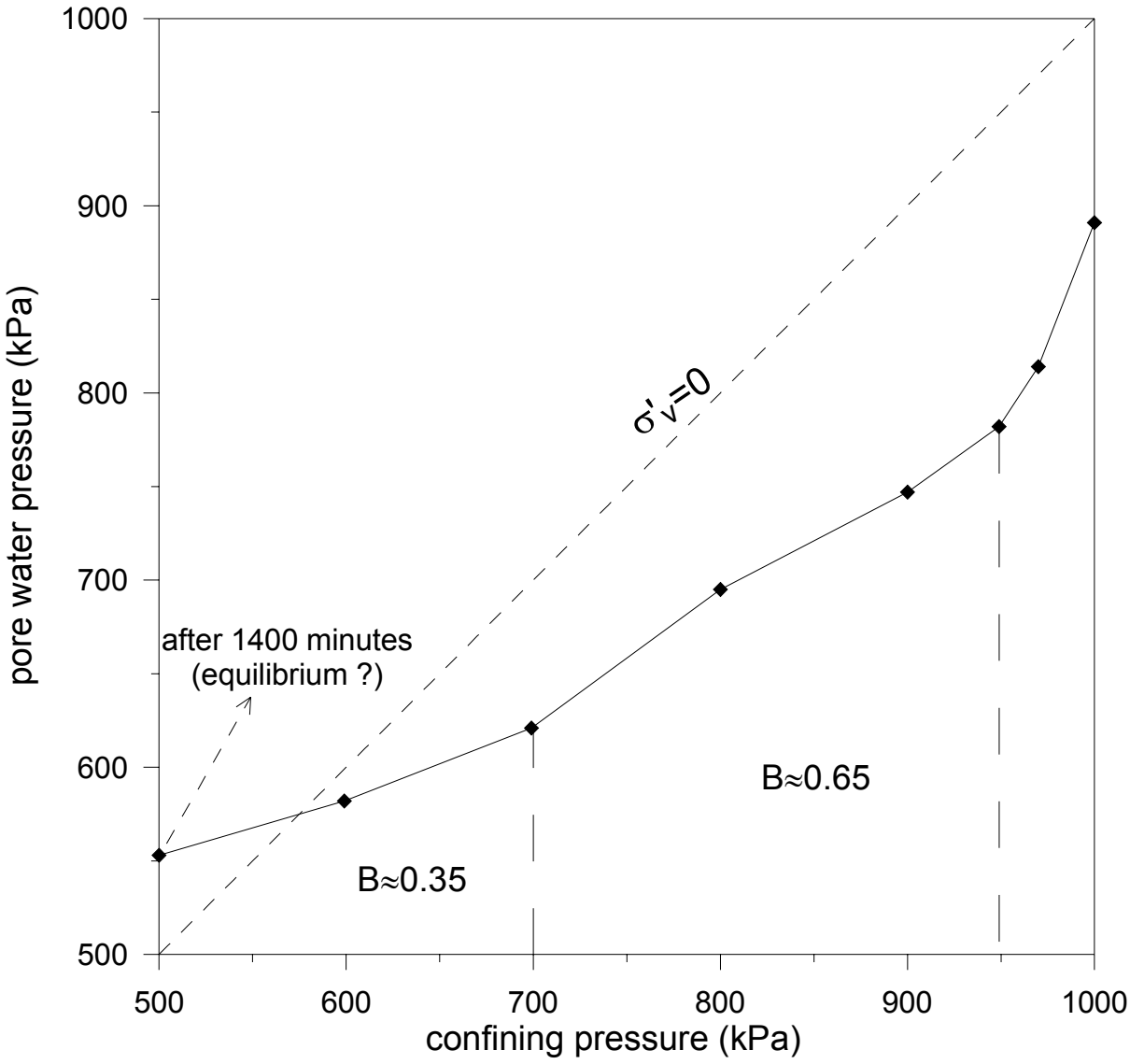

Figure 9: Evolution of pore water pressure as a function of the confining pressure during unloading at constant water content (test 5, from E to F in Figure 6)

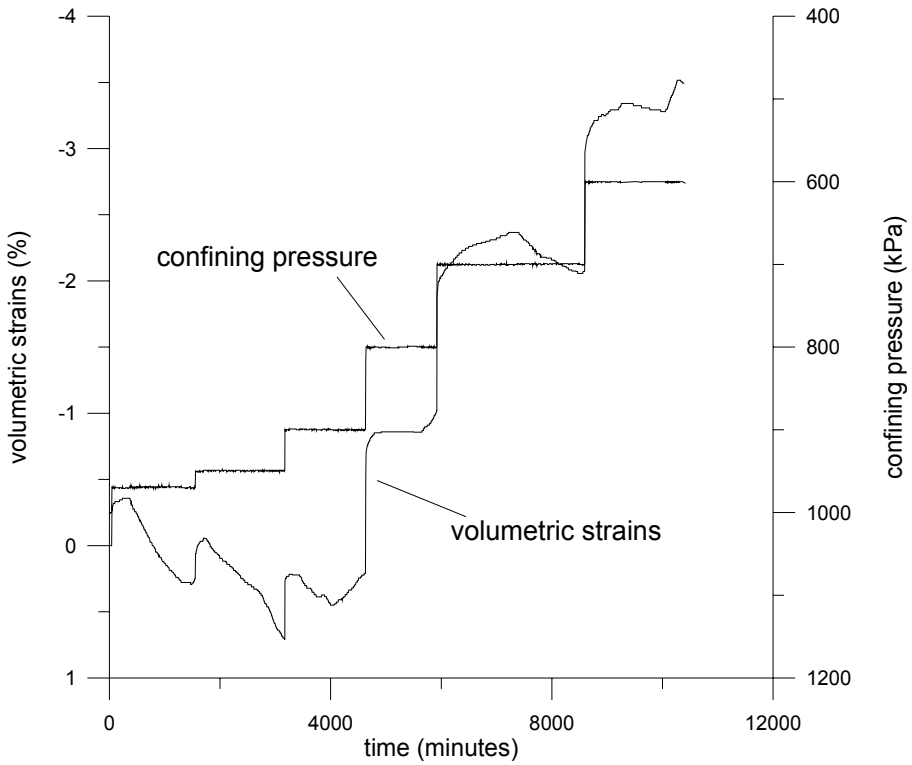

Figure 10: Volumetric strains and confining pressure versus time for different unloading steps at constant water content

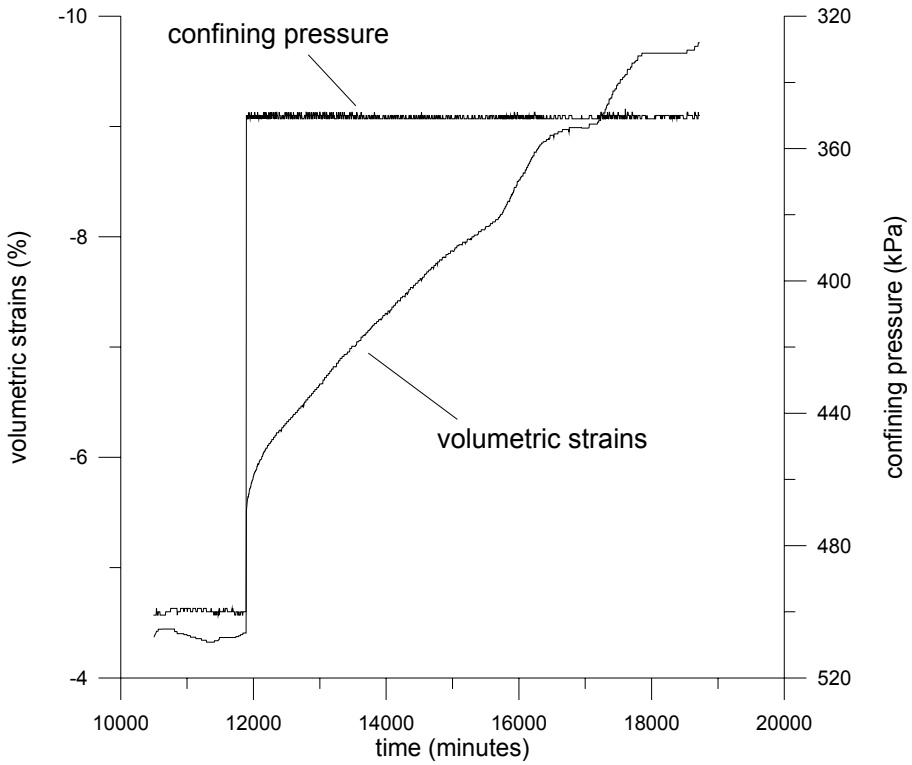

Figure 11: Volumetric strains and confining pressure versus time generated by a decrease of the confining pressure from 600kPa to 350kPa at constant water content

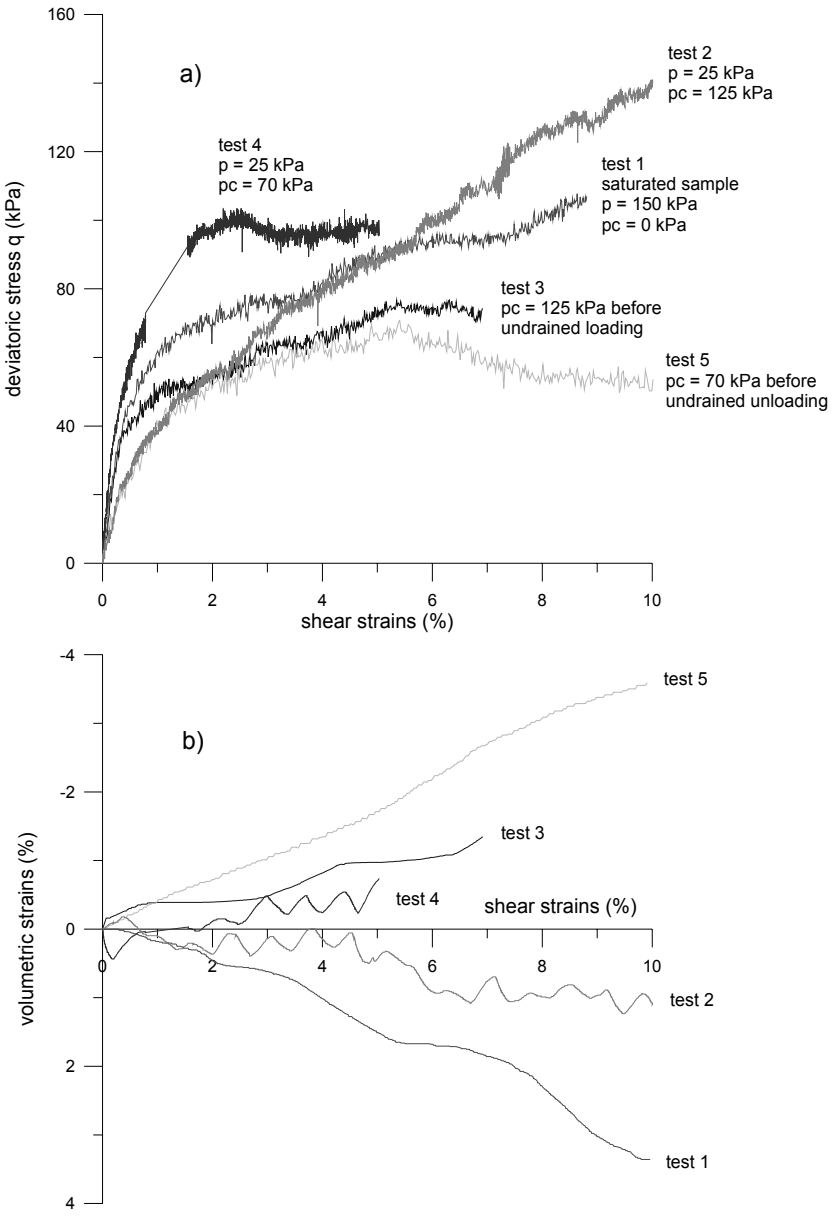

Figure 12: a) Deviatoric stress - shear strains diagram b) Volumetric strains - shear strains diagram

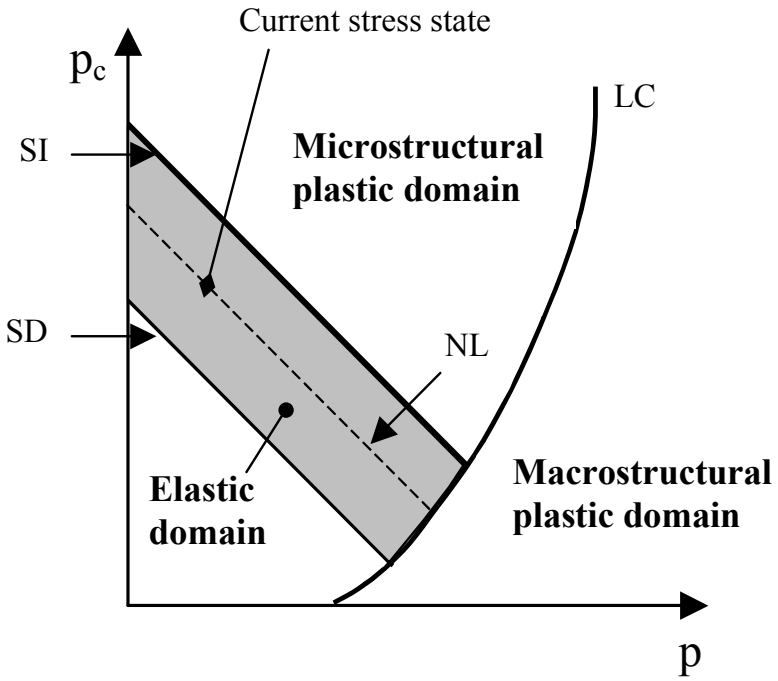

Figure 13: Yield loci in p-p_c plane (after Gens and Alonso 1992)

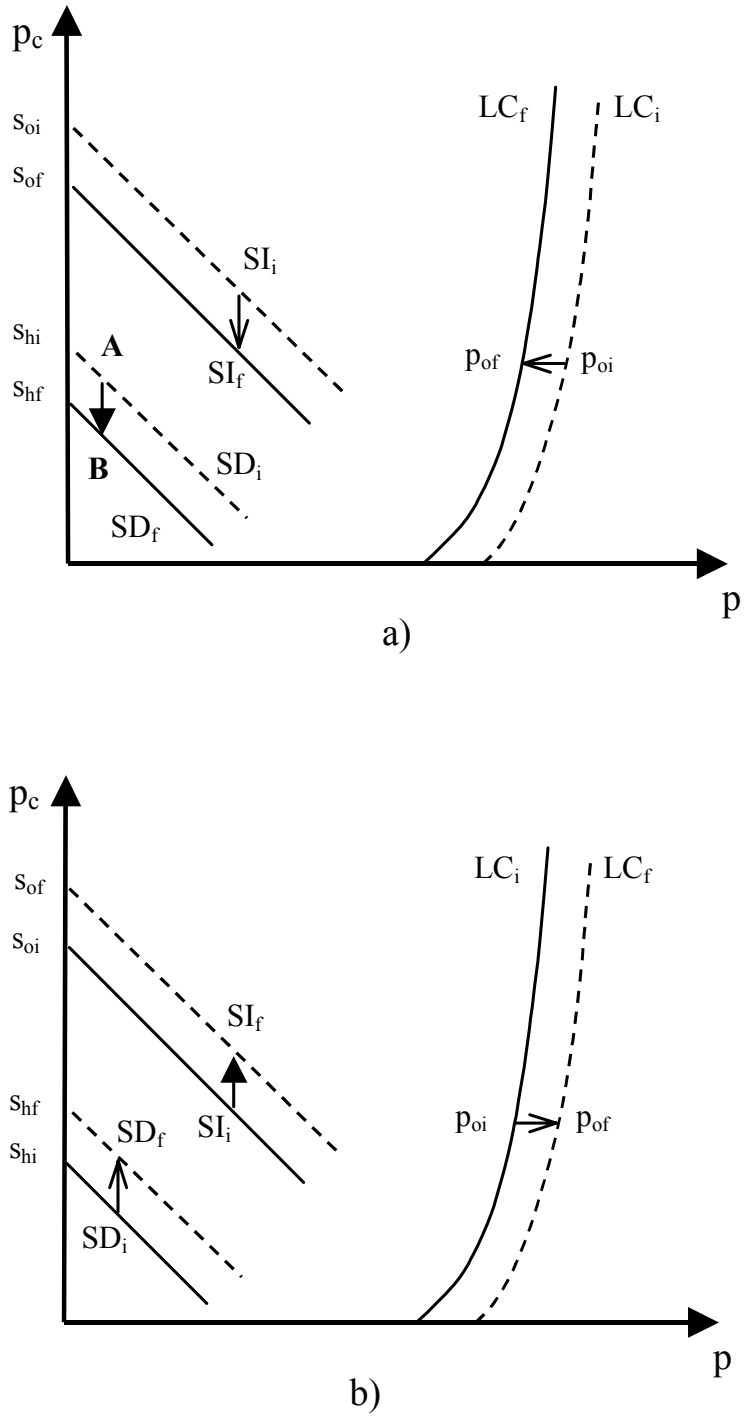

Figure 14: Coupling between microstructural and macrostructural yield curves a) With a decrease of capillary pressure – b) With an increase of capillary pressure (after Gens and Alonso. 1992)

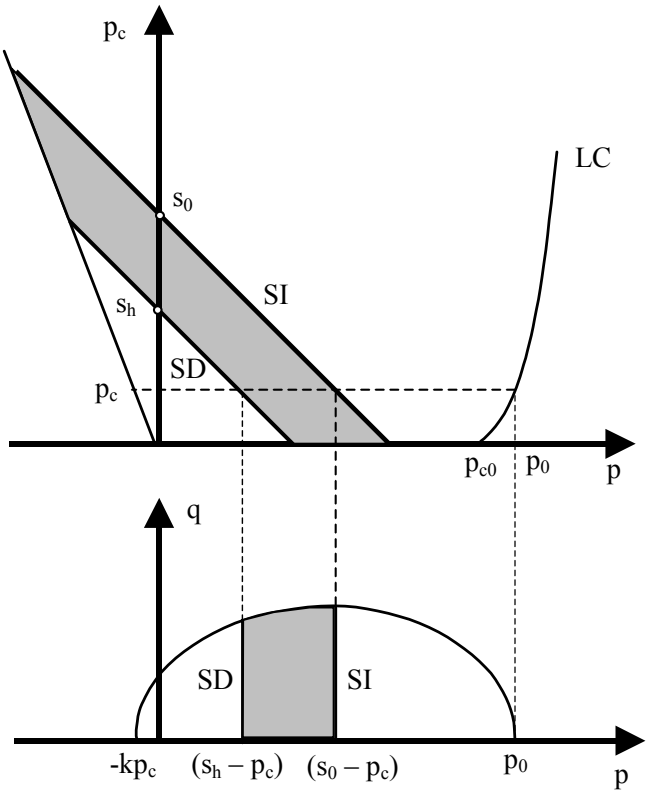

Figure 15: Yield surfaces in p-q-p_c space -a) Cross section in p-p_c plane -b) Cross section in p-q plane (after Gens and Alonso. 1992)

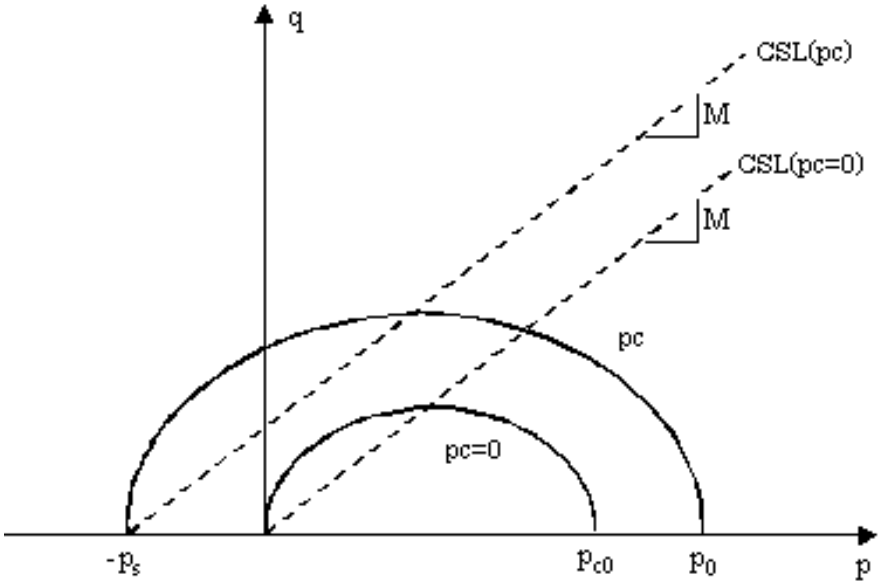

Figure 16: Position of the Critical State Line (CSL) in the p-q plane

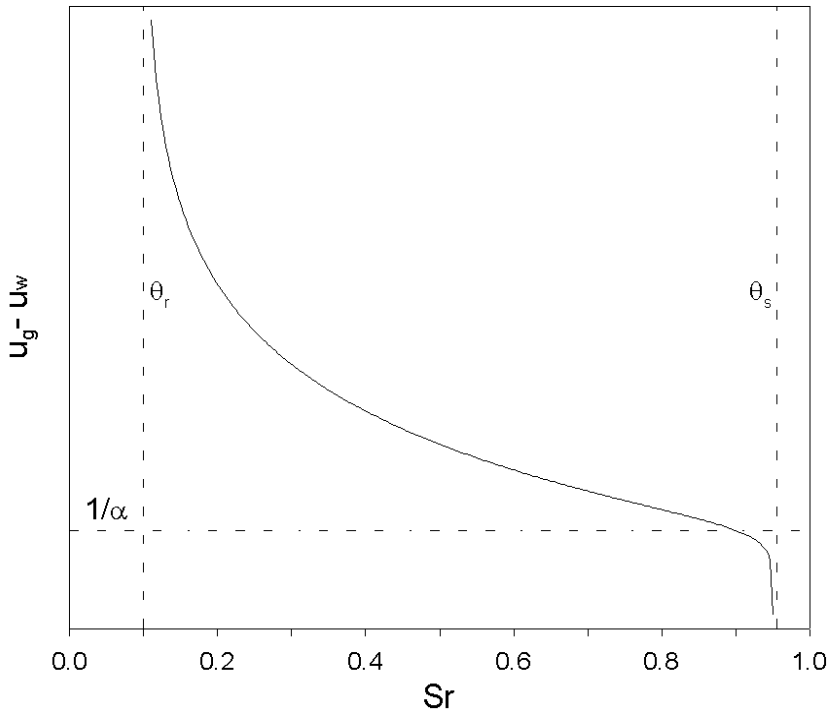

Figure 17: Parameters used in the Van Genuchten equation (Equation 16)

a)

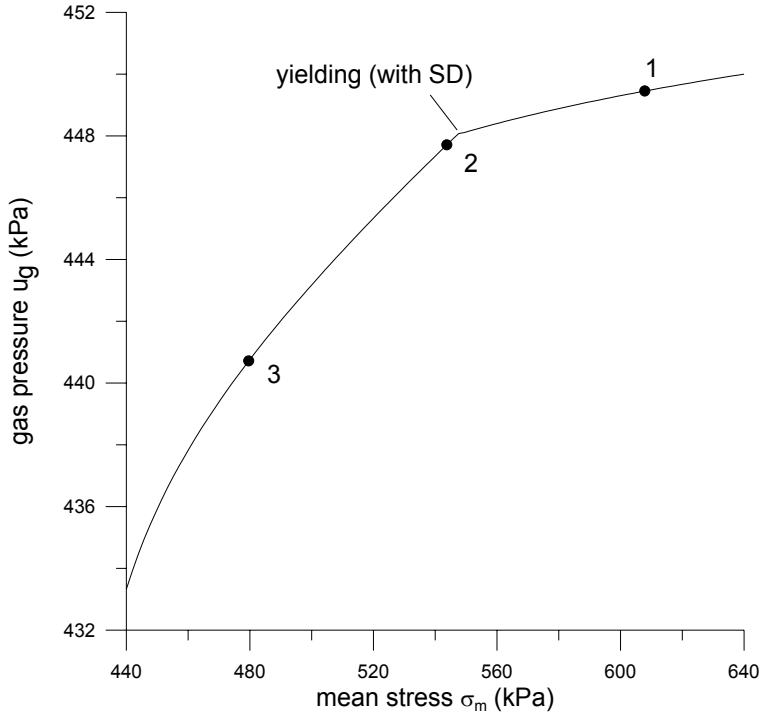

b)

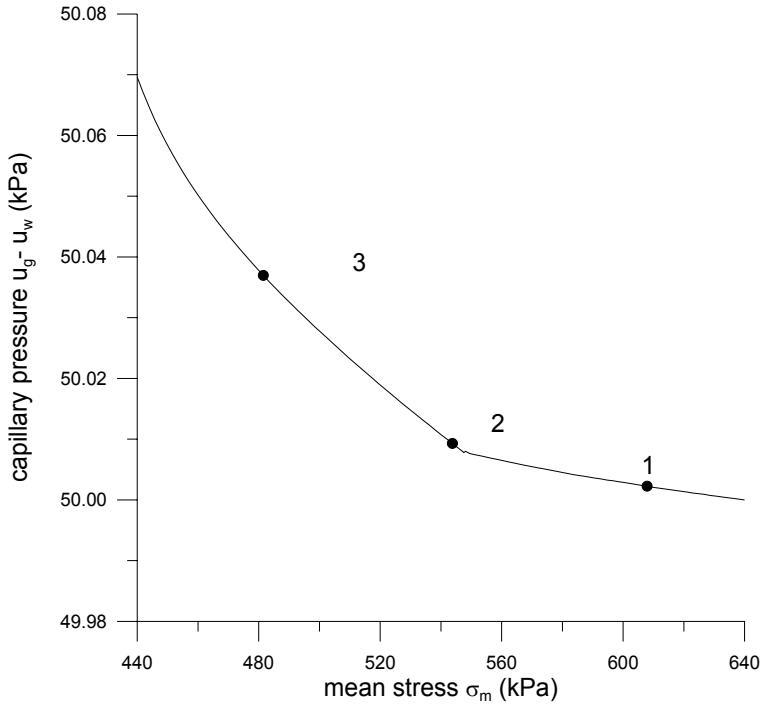

Figure 18: a) Gas pressure - mean net stress relationship b) Capillary pressure - mean net stress relationship for unsaturated soil

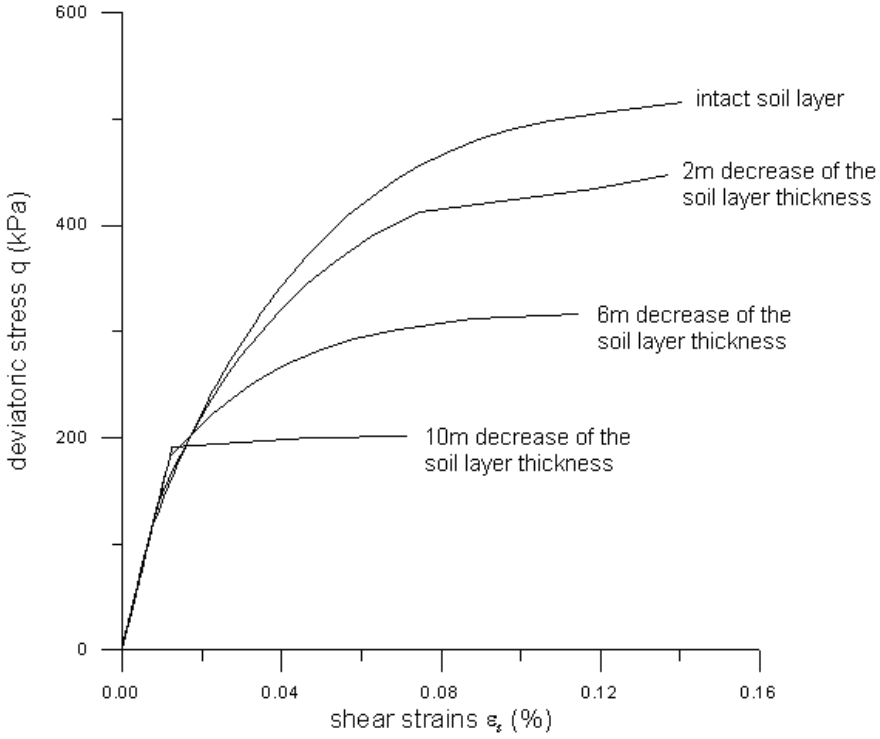

Figure 19: Shear stress-shear strains relationships under undrained conditions for an unsaturated soil